Wireless backhaul: Performance Modelling and Impact on User Association for 5G

Mona Jaber, *Student member, IEEE,* F. Javier Lopez-Martinez, *Member, IEEE,* Muhammad Ali Imran, *Senior member, IEEE,* Andy Sutton, Anvar Tukmanov, *Senior Member, IEEE,* and Rahim Tafazolli, *Senior member, IEEE*

***Abstract*—Wireless technology is the strongest contender for catering for the 5G backhaul stipulated performance where optical fibre is unavailable. In the presence of ultra-dense networks, such occurrences are exponentially increasing and different wireless technologies are investigated for this application. We present the first backhaul-specific wireless link performance modelling that considers its inherent line-of-sight nature, together with an appropriate representation of the network topology using stochastic geometry. To this end, novel tractable models are obtained to capture the performance of wireless backhaul links. These are integrated into a multi-hop hybrid backhaul performance modelling framework and are applied in the analysis of a backhaul-aware user association optimisation problem.**

***Index Terms*—Wireless Backhaul, performance, modelling, user-centric-backhaul.**

I. Introduction

5G is no longer a futuristic vision but has become today's reality and demands an imminent and efficient approach for tackling the related deployment challenges, not the least the backhaul (BH). The performance evolution of the current realistic BH towards meeting the 5G expectations is a lengthy and costly process. In a recent survey, it was found that only 3% of examined network operators are considering testing the BH network in the first trials where 68% have the radio network as priority [1]. Therefore, the BH will undergo slower evolution towards ubiquitous 5G performance. Various efforts toward bridging the BH performance gap have been recently recorded as reported in [2]. Some attempt to evolve the existing BH technologies (e.g., [3] for copper, [4] for fibre, and [5] for wireless). Others explore the integration of information technology techniques to alleviate the BH performance requirements (e.g., [6] for caching, and [7] for software defined network architectures). Theoretically, fibre is believed to be the ultimate BH solution, however, it is also known to be scarce in many 5G leading countries. In these cases, network-wide deployment is also highly impractical due to the cumbersome and very slow process of laying new fibre in urban areas. Wireless links are seen as the optimum solution to fill in the gap where fibre optic links are not available, by virtue of the minimal required installation work and relative fast deployment. Academic and industry researchers see great potential in the traditional microwave and novel extremely-high-frequency (EHF) bands and are working on evolving the technologies to meet 5G requirements. On the other hand, self-backhauling, whereby small cells re-use the radio access spectrum as means of wireless backhauling to the closest hub, is gaining more credibility with the emergence of beamforming antennas.

Wireless technology is evolving and expanding to offer fibre-like throughput in the order of few Gbps. Evolution is based on improved spectrum efficiency, e.g., high adaptive modulation, improved system gain such as multiple-input-multiple-output (MIMO) technologies and antenna array beamforming, and increased throughput efficiency with advances such as multi-layer compression schemes. Currently, the average capacity of mobile BH wireless links is less than 200 Mbps but is expected to reach beyond 10 Gbps by year 2020, partly as a result of the adopted new EHF spectrum [8]. The V-band ($71-76$ GHz and $81-86$ GHz), E-band ($57-66$ GHz), and D-band ($141-174.8$ GHz), all in the EHF category, have different spectrum characteristics and nature. The V-Band benefits from a continuous block of nine GHz and immunity to inter-link interference due to high oxygen absorption; its primary usage is envisaged to cater for the small cell last-mile BH/fronthaul. The E-Band has been regulated since year 2000 with a large amount of spectrum (10 GHz). On the contrary, it does not suffer from oxygen absorption, hence, allows longer links in the order of few kilometres. The E-band is often seen as the ultimate wireless solution where fibre is unavailable and is believed

The views expressed here are those of the authors and do not necessarily reflect those of the affiliated organisations. The authors would like to thank the UK Engineering and Physical Science Research Council (EPSRC) and BT Research and Innovation for funding this research through an Industrial Cooperative Awards in Science & Technology (iCASE) studentship. We would also like to acknowledge the support of the University of Surrey 5GIC (http://www.surrey.ac.uk/5gic) members for this work. The work of F.J. Lopez-Martinez was supported by the Spanish Government-FEDER (TEC2017-87913-R). This research was also partly funded by EPSRC Global Challenges Research Fund- the DARE project-EP/P028764/1.

M. Jaber, M.A. Imran, and R. Tafazolli are with the 5G Innovation Centre, part of the Institute for Communication Systems at the University of Surrey, Guildford,GU2 7XH, UK. e-mail:{m.jaber, m.imran, r.tafazolli}@surrey.ac.uk.

M. Jaber is also with Fujitsu Laboratories of Europe, Hayes, UB4 8FE, UK. email:m.jaber@uk.fujitsu.com

F. J. Lopez-Martinez is with Dpto. Ingenieria de Comunicaciones, ETSI Telecomunicacion, Universidad de Malaga, 29017 Malaga (Spain). (e-mail: fjlopezm@ic.uma.es)

M.A. Imran is also with the School of Engineering, University of Glasgow, Glasgow, G12 8QQ, UK. email: Muhammad.Imran@glasgow.ac.uk

A. Sutton is Principal Network Architect with BT Architecture and Technology and Visiting Professor with the School of Computing, Science and Engineering at the University of Salford, Salford, M5 4WT, UK. Email: andy.sutton@ee.co.uk

A. Tukmanov is with BT Research and Innovation, Adastral Park, Ipswich, IP5 3RE, UK. email: anvar.tukmanov@bt.com

Manuscript received July 22, 2017; accepted February 1, 2018.

to allow throughput and latency on par with fibre links. It is expected that the E-band would constitute 20% of the wireless family of mobile BH in year 2020 and the V-band 10% [8]. Simulation results in [5] demonstrate the usage of D-band over 1.2 km line-of-sight (LOS) assuming a transmit power of 10 dBm and an antenna gain of 45 dBi. While the technology is still under development, it is expected to deliver a nominal throughput in the range of 30 Gbps to 50 Gbps as the propagation in this band is not affected by oxygen absorption. The main impediment of wireless BH networks is their vulnerability to propagation conditions, not the least fading and loss of LOS. It is thus essential to derive tractable analytical models that represent the nature of wireless BH propagation with fidelity. There are emerging efforts towards addressing this need, albeit, these remain sporadic and incomplete.

A tractable approach was proposed in [9] (and used in [10]) to model the radio coverage and throughput in a cellular network, however, it does not take into account BH-specific characteristics (e.g., dominant LOS condition). Authors in [11] and [12] propose analytical models to capture the cumulative radio access and BH delay as perceived by users in the network. However, the authors consider two extreme cases; the first models the noise-limited wireless BH delay as a constant and the second models the in-band interference-limited scenario where interference is received from macro-cells and small cells. None of these assumptions fits the wireless BH characteristics as these are likely to be noise limited and are vulnerable to the fluctuations of the desired signal. The same authors propose an approximation to the noise-limited wireless BH, assuming log-normal shadowing in [13] and [14]. However, the mean packet delay is approximated by using the mean value of the link distance, instead of capturing the actual distribution of the variable distance. The availability and survivability of wireless connections are studied and modelled in [15] but do not capture the presence of dominant LOS.

In this work, we propose the first framework for analysing the performance of a wireless BH hop in LOS conditions with pertinent assumptions and tractable expressions where possible. The system model is first detailed in Section II. Accordingly, three actual performance metrics of the wireless BH family are captured: throughput, latency, and resilience in Sections III-A, III-B, and III-C, respectively. As wireless BH hops are the first contenders to spread the BH in breadth and depth in a timely manner, we next look at the impact of such hops on the end-to-end BH link performance. Accordingly, in Section IV, we model the performance of a multi-hop hybrid BH that is comprised of wireless segment(s) by employing the expressions derived in Section III. The models are used to examine and evaluate different strategies of deploying wireless hops and the impact of the fading models employed. Next, we demonstrate the usage of representative wireless BH performance models in the development and validation of new technologies. To this end, in Section V, we elaborate a BH-aware optimisation scheme which employs the proposed performance models to find the optimum association between users and cells with various BH characteristics. Section VI concludes the article.

II. System model

Typically, a wireless BH link that is properly planned, should allow for a LOS between the transmitting and receiving antennae. In addition to the dominant LOS path, a diffuse component is also present as a result of signal scattering. Such propagation is referred to as LOS-fading and is described and modelled in Section II-A.

In this work we use $\mathrm{E}\{\cdot\}$ to represent the expectation operator. The probability distribution function (pdf), the cumulative distribution function (cdf), and the complementary cdf of a random variable X are represented as $f_X(x)$, $F_X(x)$, and $\overline{F}_X(x)$, respectively. Given a function $g(x,y)$ of two random variables X and Y, $g_x(y) \triangleq g(y,x)|x$ denotes the function conditioned to a particular value x. The probability of an event z is denoted as $\Pr(z)$.

A. LOS fading representation

In a LOS-fading scenario, the diffuse component may be modelled as zero-mean Gaussian variate with variance equal to $2\sigma^2$. The sum of the dominant LOS component (with mean equal to $|\mu|$) and the diffuse component is the random variable G. The power $Z = |G|^2$ of such a signal produces Rice fading that is characterised by the Rician factor $K = |\mu|^2/2\sigma^2$ which represents the ratio between the power of the LOS component and that of the sum of the multi-path components. The cdf of the power of fading is a key expression in the derivations of performance metrics of wireless channels; in the case of Rice fading, it is represented as follows:

$$F_Z(z) = 1 - Q\left(\sqrt{2K}, \sqrt{2\frac{1+K}{\Omega}z}\right), \tag{1}$$

where, $\Omega \triangleq \mathrm{E}\{z\} = |\mu|^2 + 2\sigma^2$ and $Q(\cdot,\cdot)$ is the Marcum-Q function[1].

Clearly, analytical modelling that involves Rician fading, hence the Marcum-Q function, is mathematically very challenging. A work-around was recently proposed in [16] in which the LOS component is assumed to randomly fluctuate, i.e., $K_u = u \cdot K$, where u is a unit-mean Gamma distributed random variable with pdf given by:

$$f_U(u) = \frac{m^m \cdot u^{m-1}}{(m-1)!} e^{-m\cdot u}, \tag{2}$$

and $m \in \mathbb{N}$. This distribution was originally formulated in the context of modelling the joint effect of small-scale fading and shadowing, often referred to as *Rician shadowed distribution*. We propose to employ it in this work as a more tractable approximation to the Rician distribution owing to the additional degree of freedom, the parameter m, and we refer to is as *fluctuating Rician distribution*. In fact, it was recently demonstrated that this approximation converges to the Rician distribution as $m \to \infty$ in [17], [18]. Given that Z follows the

[1] J. Marcum, Table of Q Functions, Memorandum (Rand Corporation), Rand Corporation, 1950.

fluctuating Rician distribution, the authors derive the following simple forms of the pdf $f_Z(z)$ and cdf $F_Z(z)$, as a finite sum of powers and exponentials by restricting the parameter m to take positive integer values:

$$f_Z(z) = \sum_{i=0}^{m-1} C_i \cdot \frac{1}{B^{m-i}} \frac{z^{m-1-i}}{(m-i)!} e^{-\frac{z}{B}}, \tag{3}$$

$$F_Z(z) = 1 - \sum_{i=0}^{m-1} C_i e^{-\frac{z}{B}} \sum_{r=0}^{m-1} \frac{1}{r!} \left(\frac{z}{B}\right)^r, \tag{4}$$

with $B \triangleq \Omega(m+K)/m(1+K)$ and

$$C_i \triangleq \binom{m-1}{i} \left[\frac{m}{m+K}\right]^i \left[\frac{K}{m+K}\right]^{m-1-i}. \tag{5}$$

In this work, we use the traditional distribution of Rician fading (1) where mathematically possible, and the fluctuating Rician fading distributions (3) and (4), otherwise.

B. Backhaul Network Topology

We assume that the BH network is composed of Λ layers of nodes connected with $\Lambda - 1$ hops as in [10]. In Figure 1 (left), a BH topology that comprises two hops is shown, and (right) a simulated example of this topology that is generated using Poisson Point Process (PPP) to represent three layers: Φ_3 for the gateways in the core network, Φ_2 for the BH aggregation gateways, and Φ_1 for the small cells' layer.

The performance of a single wireless hop between layers $\kappa - 1$ and κ is then modelled assuming LOS-fading. The distribution of the distance between two layers $\kappa - 1$ and κ of the BH network is given by [10]:

$$f_X(x) = 2\pi\lambda_\kappa \cdot x \cdot e^{-\pi\lambda_\kappa x^2}, \tag{6}$$

where, λ_κ is the intensity of the PPP that represents the node distribution in layer κ in a two-dimensional plane. For the purpose of simplifying the derived expressions, in this article, we use λ to refer to λ_κ, the density of gateways in layer κ that aggregate wireless BH links from layer $\kappa - 1$. Although the models derived account for parallel links, these are considered as alternative hot-backup connections, thus, do not allow simultaneous transmission. As such, the throughput derivations assume one active link, hence the scheduling delay is not considered. Nonetheless, the topology and redundancy schemes are captured in the resilience modelling derivations.

Wireless point-to-point BH deployments are often noise limited, i.e., the interference from neighbouring links within the designated spectrum is minimal, thus, the signal-to-noise-and-interference ratio (SINR) can be approximated with a signal-to-noise-ratio (SNR). Indeed, the traditional wireless spectrum is licensed and careful frequency planning limits inter-link interference. On the other hand, in-band backhauling is enabled through the usage of beamforming antennae which, by virtue, limit the inter-beam interference [19]. Moreover, the propagation characteristics of the EHF waves suppress unwanted signals from neighbouring links, naturally. For these reasons, the received SINR of wireless links in any of the mentioned bands can be approximated with the SNR. The instantaneous SNR at the receiver side, denoted as γ, can be expressed as:

$$\gamma(h, x) = \frac{P \cdot A \cdot h \cdot x^{-\alpha}}{L_0 \cdot N}, \tag{7}$$

where, L_0 is the propagation loss constant, α is the propagation exponent, x is the propagation distance of the signal, h represents the random component of small-scale fading, P is the equivalent isotropic radiated power (EiRP), A is the receive antenna gain, and N is the thermal noise power. Note that we explicitly indicate the dependence of γ on h and x, although for the sake of notational simplicity we will simply refer to γ unless necessary to avoid any confusion.

Given that a wireless BH is an inherently LOS-based transmission, we assume that the distribution of h is that of a Rician-distributed fading channel. Thus, assuming a normalized channel $\mathrm{E}\{h\} = 1$, the distribution of the instantaneous SNR conditioned to a particular value of x, denoted as $\gamma_x \triangleq \gamma(h, x)|x$, follows a power Rician distribution, as in Section II-A, with mean $\Omega_x = P \cdot A \cdot x^{-\alpha}/L_0 \cdot N$ (replacing h by $\mathrm{E}\{h\} = 1$ in (7)) .

III. Wireless Backhaul Performance

A. Throughput

The upper bound of a wireless channel capacity (in symbols per second) depends firstly on the channel bandwidth (W) and the SNR. The actual bit-per-second throughput is derived from the selected modulation and coding scheme which relates to the number of bits per symbol. Higher modulation schemes require higher SNR in order to avoid bit confusion which would lead to unwanted high bit error rates. Defining $T_x \triangleq W \cdot \log_2(1 + \gamma_x)$, then the average rate for a given value of x can be derived as follows, by using the definition of the expectation operator:

$$\mathrm{E}\{T_x\} = \int_0^\infty W \cdot \log_2(1 + \gamma_x) \cdot f_{\gamma_x}(z) dz. \tag{8}$$

Theorem 1: The average capacity of a wireless link under Rician fading at a given distance x can be expressed as follows:

$$\mathrm{E}\{T_x\} = \frac{W}{\ln(2)} e^{-K} \sum_{n=0}^{\infty} \frac{K^n}{n! \cdot n!} \times G_{2,3}^{3,1}\left[\frac{(1+K)}{\Omega_x} \,\middle|\, \begin{matrix} 0, 1 \\ n+1, 0, 0 \end{matrix}\right], \tag{9}$$

where, $G_{p,q}^{m,n}[\cdot]$ is the Meijer-G function [20, 9.301].

Proof: The proof is provided in Appendix A.

Even though the expression in (9) can be computed with state-of-the-art mathematical packages such as Mathematica[2], it necessitates, nonetheless, the evaluation of an infinite series expression involving the unwieldy Meijer-G function. To this end, we propose the usage of the fluctuating Rician approximation, presented in Section II-A, in order to reduce the complexity of computation, and as will be later shown, to facilitate further analytical derivations.

Theorem 2: The average capacity of a wireless link under

[2]https://www.wolfram.com/mathematica/

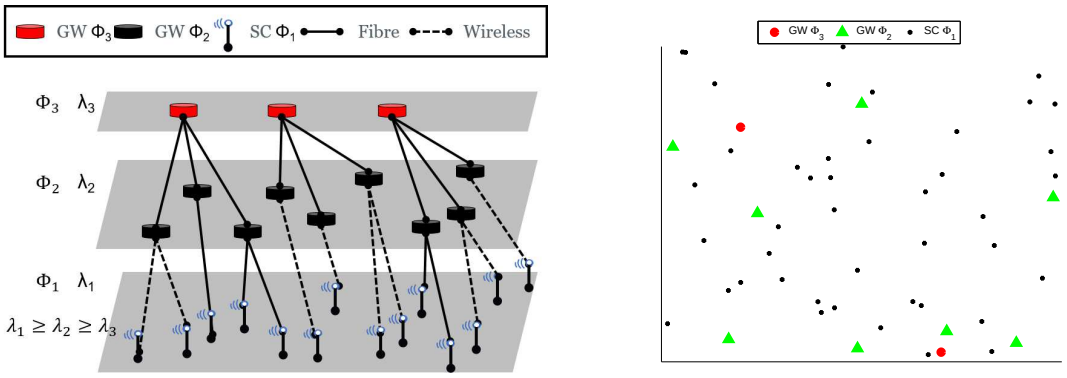

Fig. 1. Example of multi-hop hybrid BH network modelled using PPP.

Rician fading at a given distance x can be approximated as follows, using the fluctuating Rician fading pdf (3):

$$\mathrm{E}\{T_x\} \approx \mathrm{E}\{T'_x\} = \frac{W}{\ln(2)} e^{1/B_x} \sum_{i=0}^{m-1} C_i \sum_{l=0}^{m-i-1} \frac{\Gamma(-l, 1/B_x)}{B_x^l}, \tag{10}$$

where, $B_x \triangleq \Omega_x(m+K)/m(1+K)$ and $\Gamma(\cdot,\cdot)$ is the upper incomplete Gamma function, which can be computed in this specific case as [20, eq. (8.352.3)]:

$$\Gamma(-n, x) = \frac{(-1)^n}{n!} \left[E_1(x) - e^{-x} \sum_{r=0}^{n-1} (-1)^r \frac{r!}{x^{r+1}} \right], \tag{11}$$

where, $E_1(\cdot)$ is the exponential integral function.

Proof: The proof is provided in Appendix B.

For sufficiently large m, the Fluctuating Rician distribution collapses to the Rician distribution as shown in [18] (please refer to Figure 1 [18]). This is illustrated in Table I, where we first find the value of m that would yield approximated results (10) within $\epsilon = 0.1\%$ of those obtained with (9) for different values of K and α ($\epsilon = (\mathrm{E}\{T'_x\} - \mathrm{E}\{T_x\})/\mathrm{E}\{T_x\}$). With the selected value of m, the approximation using (10) is validated for a given wireless BH with different values of K, as shown in Figure 2.

The expected throughput over all possible values x is $\mathrm{E}\{T\}$, which can be derived as follows and approximated using (10):

$$\mathrm{E}\{T\} = \int_0^\infty T_x \cdot f_x(x) dx$$
$$\approx \frac{W}{\ln(2)} \sum_{i=0}^{m-1} C_i \sum_{l=0}^{m-i-1} \int_0^\infty e^{x^\alpha/B} x^{\alpha \cdot l} \frac{\Gamma(-l, x^\alpha/B)}{B^l} 2\pi\lambda \cdot x \cdot e^{-\pi\lambda x^2} dx \tag{12}$$

where, $B \triangleq \frac{m+K}{m(K+1)} \frac{P \cdot A}{L0 \cdot N}$. The expression still requires numerical integration but can be solved with, relatively, manageable complexity. However, for the special case of $\alpha = 2$, we can further simplify the expression to a closed form.

Theorem 3: The average capacity of a wireless link under Rician fading at any distance and for a special case of $\alpha = 2$ can be approximated as in (13) on the next page.

Proof: The proof is provided in Appendix C.

The expression (12) is used in Figure 3 to derive the average throughput over a range of gateway densities for two settings of the propagation exponent: $\alpha = 2.5$ and $\alpha = 3$. As can be expected, higher gateway densities indicate shorter wireless BH ranges, consequently, higher γ and higher throughput. Similarly, a higher propagation exponent induces higher loss per decade, hence, lower achievable throughput, as seen in Figure 3.

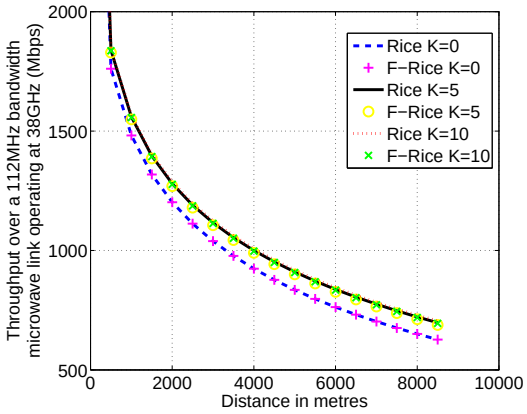

Fig. 2. Optimum setting of m is used to generate approximated throughput within 0.1% error of the actual throughput using Rice fading for three values of K and $\alpha = 2.5$. (Refer to Table I).

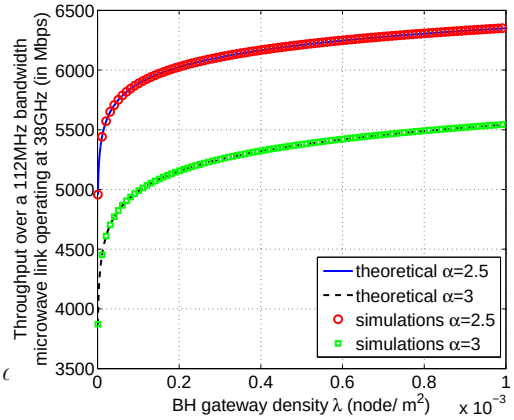

Fig. 3. Average throughput over any distance using the proposed approximation (10) with m values as defined in Table I.

TABLE I
(LEFT) DEFAULT PARAMETERS USED IN ALL FIGURES, UNLESS OTHERWISE STATED. (RIGHT) MINIMUM VALUE OF m REQUIRED TO REDUCE THE ERROR OF APPROXIMATION.

Parameter	Value
Rice factor (K)	10
Channel bandwidth (W) in MHz	112
Propagation exponent (α)	2.5
Operating frequency (f) in GHz	38
Propagation loss constant	dB
$\left(L_0 = 10\alpha \log_{10}(4\pi/\mathbf{c}^{\mathrm{m/s}}) + 10\alpha \log_{10}(f^{\mathrm{GHz}})\right)$	80.0468
Equivalent isotropic radiated power (EiRP P) in dBm	20dBm+43dBi
Receive antenna gain (A) in dBi	43
Thermal noise power (N) in mW/MHz	$4 \cdot 10^{-12}$

K	α=2	α=2.5	α=3
0	1	1	1
1	4	5	8
5	15	19	28
10	15	20	30
20	15	20	30

$$\mathrm{E}\{T\} \approx \frac{W}{\ln(2)} \sum_{i=0}^{m-1} C_i \sum_{l=0}^{m-i-1} \pi\lambda B \frac{(-1)^l}{l!} \times \left\{ \frac{\Gamma(l+1)}{l+1} {}_2F_1\left(l+1, l+1; l+1; 1-\pi\lambda B\right) - \sum_{r=0}^{l-1} (-1)^r r! (\pi\lambda B)^{r-l} (l-r-1)! \right\}. \tag{13}$$

$$\Pr\{\gamma > \tau\} = \int_0^\infty Q\left(\sqrt{2K}, \sqrt{2(1+K)\frac{\tau N L_0 x^\alpha}{PA}}\right) 2\pi\lambda \cdot x \cdot e^{-\pi\lambda x^2} dx \tag{14}$$

$$\begin{aligned} \Pr\{\gamma_{\alpha=2} > \tau\} &= \int_0^\infty Q\left(\sqrt{2K}, x \cdot \sqrt{2(1+K)\frac{\tau N L_0}{PA}}\right) 2\pi\lambda \cdot x \cdot e^{-\pi\lambda x^2} dx \\ &= 1 - \frac{(1+K)\tau N L_0}{(1+K)\tau N L_0 + \pi\lambda PA} \times \exp\left(-\frac{\pi\lambda K PA}{(1+K)\tau N L_0 + \pi\lambda PA}\right) \end{aligned} \tag{15}$$

B. Latency

Latency in a communication system is a combined result of four distinct processes: propagation, transmission, processing, and queuing. The propagation delay is the time it takes a packet to travel between transmitting and receiving antennae, hence, it can be ignored in wireless communication as the propagation speed is equal to speed of light. The transmission delay is the time taken to push all the packet bits onto the link. The dominant factor causing transmission delays in wireless links is the decode-and-forward mechanism, typically applied at each hop, which results in retransmissions when the received SNR value is below the required threshold (τ). Accordingly, the success transmission probability of one hop in a wireless point-to-point link is equivalent to the probability $\Pr(\gamma > \tau)$ which can be directly obtained from (1) as $1-F_Z(z)$ for Rician fading, at a given distance. Accordingly, the average success probability over all possible values of x, can be obtained as in (14). For a special case in which $\alpha = 2$, a closed form solution for (14) can be obtained using [21, eq. B.27], as shown in (15). Considering a timeslotted transmission over wireless BH links, let θ be the timeslot duration corresponding to given wireless technology. If the first attempt of transmission is successfully received, the transmission delay would be equal to θ, which is the ideal case. Otherwise, retransmissions occur until a successful reception is recorded. Each retransmission would incur an additional delay equal to the timeslot duration, if we assume an ideal error-less reception of acknowledgment in the opposite direction. For instance, if the probability of successful reception is 0.5, the expected latency over the wireless hop would be $2\times\theta$. In general, the mean transmission delay is inversely proportional to the transmission success probability $\Pr(\gamma > \tau)$, following the approach in [13], as shown here:

$$\mathrm{E}\{D^t\} = \frac{\theta}{\Pr\{\gamma > \tau\}}. \tag{16}$$

Figure 4 shows the average success probability of transmission over a wireless link for a range of SNR target values, four node densities, and two propagation exponents $\alpha = 2.5$ and $\alpha = 3$. For $\alpha = 2.5$, the success probability is quasi-guaranteed (to the tenth significant digit). For the latter setting ($\alpha = 3$), the success probability is predominantly constrained by the propagation, but is also limited by node density and setting of τ. For a high setting of $\theta = 100$ μsec, the transmission delay associated with a high SNR target $\tau = 15$ dB and for $\alpha = 3$ and $\lambda = 1$ gateway per km^2, the effective transmission delay would be ~ 103.1 μsec.

In addition to the transmission delay, communication over wireless links requires node processing which incurs additional delays. These are the processing and queuing delays which are often approximated jointly as a Gamma distribution with parameters that depend on the router, the given load, and

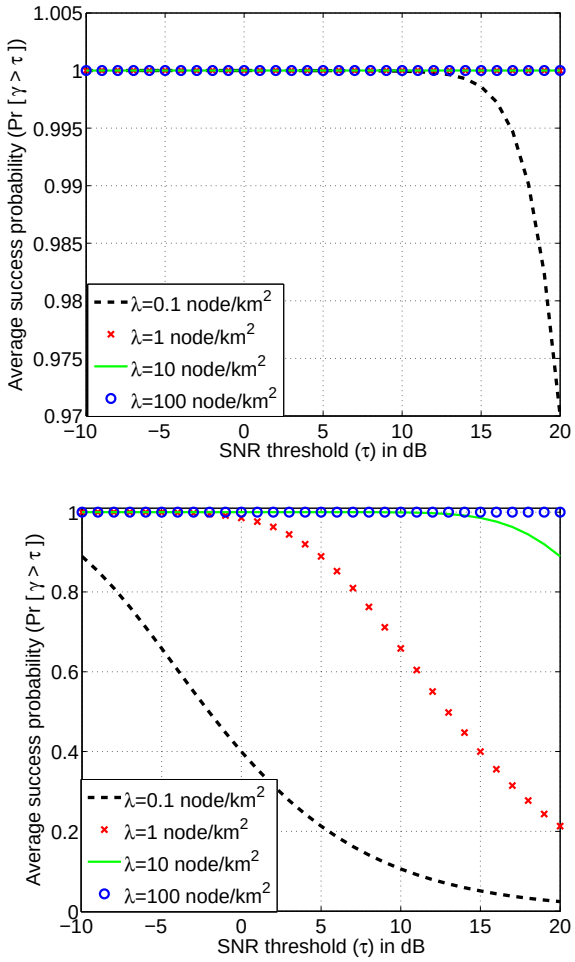

Fig. 4. The average transmission success rate over a wireless link with Rice fading and variable distance is shown for two propagation exponents $\alpha = 2.5$ (top) and $\alpha = 3$ (bottom) for $\lambda = \{0.1, 1, 10, 100\}$ gateway(s) per km^2. Parameters settings are as listed in Table I except $P = 10 + 43$ dBm as for higher values the success probability is $> 99.999\%$.

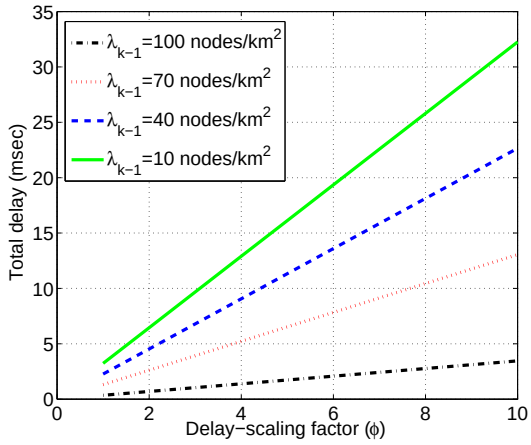

Fig. 5. The expected total delay over a wireless link is represented in this figure variable node delay-scaling factor and node density. Parameters based on Table I with P=100 mW, $\mathrm{E}\{\epsilon\}$=1500 bits, a=10 μsec, b=0.01 μsec/bit, τ=10 dB, λ_k=1 node/km^2.

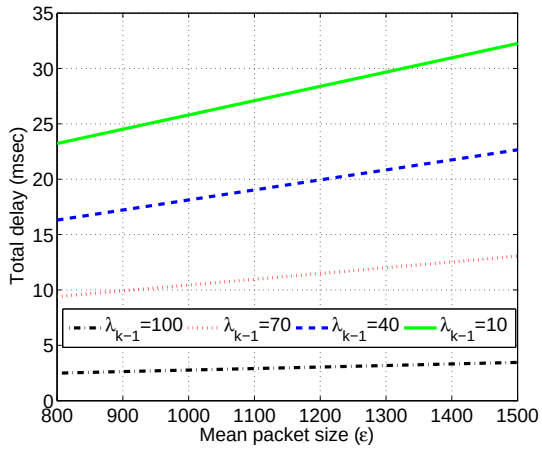

Fig. 6. The expected total delay over a wireless link is represented in this figure for variable packet length (in bits) and node density. Parameters based on Table I with P=100 mW, ϕ=10, a=10 μsec, b=0.01 μsec/bit, τ=10 dB, λ_k=1 node/km^2.

technology as in [14]:

$$\mathrm{E}\{D^{r,q}\} = \phi \cdot (1 + 1.28 \cdot \lambda_{k-1}/\lambda_k) \cdot (a + \mathrm{E}\{\epsilon\}b), \quad (17)$$

where, ϕ is a delay-scaling factor that reflects the processing power of the node per connected line; higher values of ϕ incur higher delays. The expression $(1+1.28\cdot\lambda_{k-1}/\lambda_k)$ denotes the mean number of nodes in layer $k-1$ served by the designated node (router) in layer k to which the wireless BH link in connected. The parameter a (in μsec) represents the traffic-independent processing delay of the router, and b (in μsec/bit) represents the processing delay with respect to the packet size $\mathrm{E}\{\epsilon\}$. Accordingly, a point-to-point wireless link using decode-and-forward scheme incurs a total delay D, as shown below:

$$\mathrm{E}\{D\} = \mathrm{E}\{D^t + D^{r,q}\} = \mathrm{E}\{D^t\} + \mathrm{E}\{D^{r,q}\},$$
$$= \frac{\theta}{\mathrm{E}\{\Pr(\mathrm{SNR} > \tau)\}} + \phi \cdot \left(1 + 1.28 \cdot \frac{\lambda_{k-1}}{\lambda_k}\right) \cdot (a + \mathrm{E}\{\epsilon\}b). \quad (18)$$

Figures 5 and 6 show that the number of connected lines (function of $\lambda_{\kappa-1}$) has a major impact on increasing the processing delay (hence, the total delay). The total delay also seems to increase linearly with increasing delay-scaling factor (ϕ), as shown in Figure 5. The delay also increases with increase in packet length, as seen in Figure 6, but the end-value is dominated by the effect of the delay-scaling factor and node density. Results shown in both figures advocate that the joint processing and queuing delay (tens of msec) is orders of magnitude higher than the transmission delay in wireless BH links (~ 0.1 msec).

C. Resilience

There are several performance metrics that may be used to characterise the resilience of a link [15]. (i) Reliability is the probability of a link being operational and is measured as the mean time before failure (MTBF). (ii) Survivability measures the performance of recovering from failure in terms of the mean time to repair (MTTR). (iii) Availability is the proportion of time the link is operational but, differently from

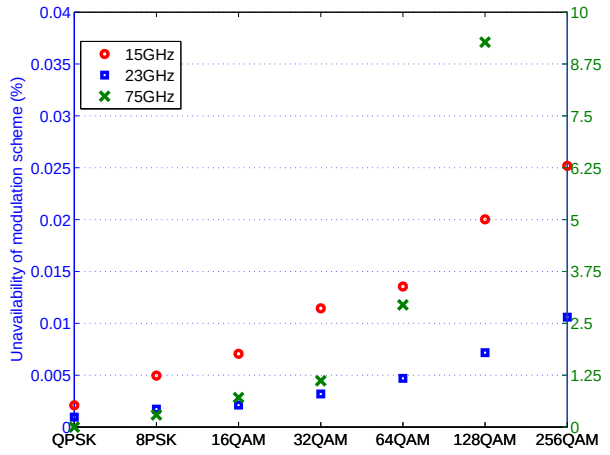

Fig. 7. Percentage of time the indicated ACM is not available for three scenarios based on data from different trials using automatic coding and modulation in different frequency bands.

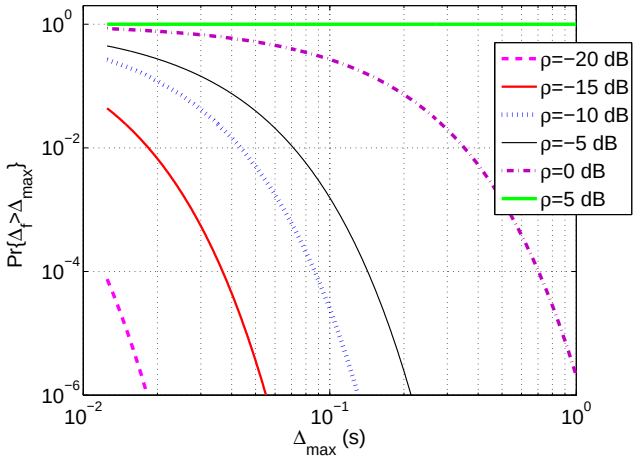

Fig. 8. Outage probability of a Rice fading channel link based on (21), assuming $f_m = 10$ Hz for different values of ρ. Other parameters used in the simulations are listed in Table I.

(i), it takes into account failures and repair; it is quantified as uptime/(uptime+downtime) e.g., MTBF/(MTBF+MTTR). In this paper, we model the outage probability, i.e. downtime/(uptime+downtime) which is affected by the radio link failure and the equipment failure. Features such as automatic coding and modulation (ACM) are commercially employed to increase the robustness of the radio link at the cost of spectrum efficiency reduction. Figure 7 shows experimental results that highlight the vulnerability of EHF signals to fades and weather conditions [22] [5].

In this case, mechanisms such as decode-and-forward dampen the effect of loss of radio link through repeated retransmissions. These improve the tolerance of a wireless link which may be recovered if the fade lasts less than the time allowed for maximum retransmission.

Consequently, modelling the resilience of a wireless link entails an analysis of the fade duration distribution and determining the probability of having a fade duration that is less than the critical limit. The average receive power is characterized by $\mathrm{E}\{J\}$, and the minimum power level threshold is $J_{\min}$ (e.g., receiver sensitivity or minimum received signal strength to guarantee a target bit error rate). The fading margin is defined as $\rho \triangleq \sqrt{J_{\min}/\mathrm{E}\{J\}}$ which is equal to $\sqrt{J_{\min}}$ for $\mathrm{E}\{J\} = 1$. The time during which the signal power is below $J_{\min}$ is the fade duration. The first step is to determine the level crossing rate R_L and the average fade duration $\mathrm{E}\{F_d\}$, equivalent to mean-time-to-repair or MTTR. These are derived in [23] for Rician fading, as shown below:

$$R_L = \sqrt{2\pi(K+1)} \cdot f_m \cdot \rho e^{-K-(K+1)\rho^2} \cdot I_0(2\rho\sqrt{K(K+1)}) \quad (19)$$

$$\mathrm{E}\{F_d\} = \frac{1 - Q(\sqrt{2K}, \sqrt{2(K+1)\rho^2})}{\sqrt{2\pi(K+1)} \cdot f_m \cdot \rho e^{-K-(K+1)\rho^2} \cdot I_0(2\rho\sqrt{K(K+1)})} \quad (20)$$

where, $f_m = vf/\mathfrak{c}$ is the maximum Doppler shift, v denotes the relative motion of scattering objects between the transmit and receive antennae, f is the carrier frequency of the signal, and $\mathfrak{c}$ is the speed of light and K is the Rice factor.

The none-fade duration $\mathrm{E}\{\overline{F_d}\} = 1/R_L - \mathrm{E}\{F_d\}$ (equivalent to the MTBF) is then defined and used in a Gilbert-Elliot two-state-model to find the probability of fades being larger than a threshold $J_{\min}$ as in [15]. Owing to the re-transmissions mechanism, such fades do not necessarily cause a link outage unless they persist for a duration $\Delta_f > \Delta_{\max}$. The outage probability of a wireless link is thus $\Pr(\Delta_f > \Delta_{\max})$ which can only be determined if the fade duration distribution is known. Albeit, this distribution is largely unknown and remains an open problem in the literature ever since the original formulation by Rice [24]. In this work, we assume that the fade duration distribution exhibits an exponential-like behaviour for high values of ρ, similar to [25]. The radio outage probability of a wireless BH link, ($\mathrm{E}\{O^r\}$), can thus be expressed as follows:

$$\mathrm{E}\{O^r\} = \Pr(\Delta_f > \Delta_{\max}) = e^{-\frac{\Delta_{\max}}{\mathrm{E}\{F_d\}}}. \quad (21)$$

In Figure 8, the radio outage probability (i.e., $\mathrm{E}\{O^r\}$) of a wireless link that follows Rician fading is simulated as a function of the critical time $\Delta_{\max}$ and the fade margin ρ. Higher values of $\Delta_{\max}$ improve the radio link availability and vice-versa. On the other hand, higher fade margins render the probability of fades higher, consequently, the link is more vulnerable which increases the outage probability.

Often, key radio links that affect a large service area are designed with redundancy schemes that employ at least two independent radio links, such as [1+1] or [2+0] schemes. In the former example, one link is active at a given time with seamless switching to the backup link in case the first is in outage. In the latter example, both links are used simultaneously to enhance the effective throughput; if one radio link fails, the system switches to a single link automatically without causing service interruption. In both examples, the wireless connection is only in outage if both radio links fail simultaneously. In mesh wireless networks, there are often more than one path between two points; these points are considered disconnected if all possible paths fail simultaneously. The outage expression, with any redundancy scheme, can be extended as follows,

according to (21):

$$\mathrm{E}\{O^{r'}\} = \mathrm{Pr}'(\Delta_f > \Delta_{\max}) \overset{(a)}{=} \prod_i^L e^{-\frac{\Delta_{\max}}{\mathrm{E}\{F_{d,i}\}}} \overset{(b)}{=} e^{-L\frac{\Delta_{\max}}{\mathrm{E}\{F_d\}}} \tag{22}$$

where, L denotes the number of links and $\mathrm{E}\{F_{d,i}\}$ is the mean fading duration over link i. The equality (a) indicates that, in case parallel links are used as backup between layers $\kappa - 1$ and κ, the outage occurs only when all the links fail simultaneously. The notation Pr' refers to the link outage probability with redundancy deployments. If the same value can be assumed for the mean fading duration of all L links, then the expression is further simplified as in ((b)-22) [15].

Equipment failure is another reason for wireless link outages, and concerns both indoor units (IDUs) and outdoor units (ODUs). The MTBF of such units is normally very high ($>$ 12years) and redundancy schemes are often used to improve the reliability. As such, a unique wireless link could be equipped with an active ODU and a hot-backup passive ODU that is activated whenever the prime ODU fails. The MTTR for wireless equipment varies significantly based on the location and accessibility; in an urban environment, it is often within three hours but may take up to three days in remote areas with difficult access. The outage probability of wireless links, including radio equipment and radio link failures, and any redundancy plan can be expressed as follows:

$$\begin{aligned}\mathrm{E}\{O\} &\triangleq 1 - \mathrm{E}\{(1 - O^{r'}) \times (1 - O^{o'}) \times (1 - O^{i'})\} \\ &\overset{(a)}{=} 1 - (1 - \mathrm{E}\{O^{r'}\}) \times (1 - \mathrm{E}\{O^{o'}\}) \times (1 - \mathrm{E}\{O^{i'}\})\end{aligned} \tag{23}$$

where, $O^{o'}$ and $O^{i'}$ are the outage probabilities of outdoor units and indoor units, respectively, such that $O^{o'} \triangleq \prod_i O_i^o$, where, i indicates the redundancy index of the hardware, and $O_i^o \triangleq (\mathrm{MTTR}/(\mathrm{MTBF} + \mathrm{MTTR}))_i^o$ is the outage probability of the outdoor unit with redundancy index i based on the MTTR and MTBF values. The equality (a) in (23) is possible because the concerned probabilities are independent of each other.

The cause of a wireless link outage is often the radio failure, as shown in Figure 9, unless the fade margin is very low. For these low values, the wireless link outage probability is dominated by equipment failure. For higher fade margin values, the ODU and/or IDU failures have limited impact on the total wireless link availability.

IV. Wireless BH in a Multi-hop-hybrid Network

In this section, we integrate the derived performance models of a wireless BH hop in the estimation of the multi-hop hybrid BH performance. Referring to the topology in Figure 1, with parameters as defined in Table II, we derive the expectations of the holistic BH resilience, capacity, and latency following the approach in [10]. Based on [10], the resilience of a multi-hop BH is affected by outages on any hop. Differently, the capacity of a multi-hop hybrid BH is determined by the single hop which is the most limiting, i.e., the last-mile. The latency, on the other hand, is the aggregate effect of delay occurring on all hops. We consider that the BH network between the

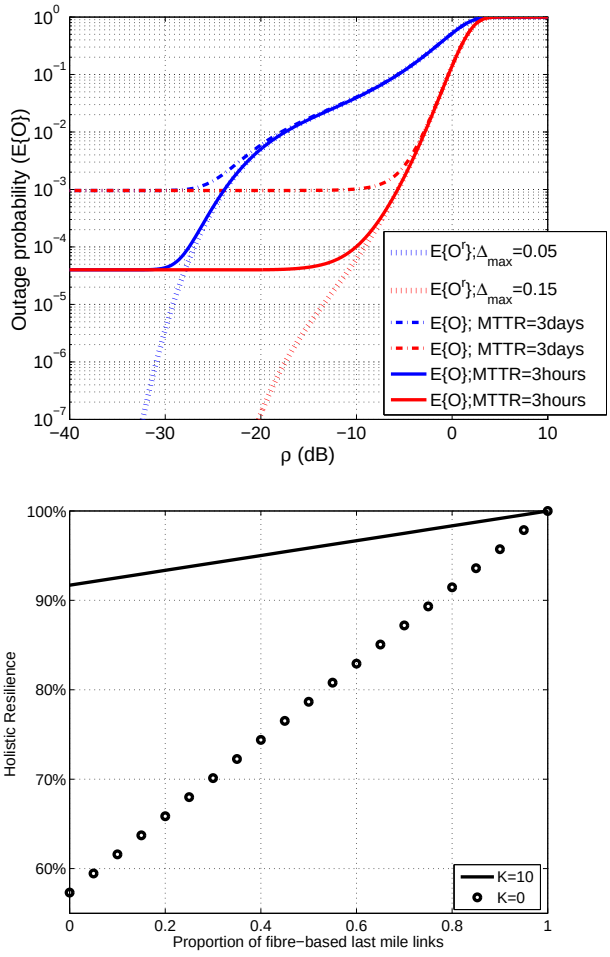

Fig. 9. (Top) The outage probability of the wireless link is shown as a function of ρ for two values of $\Delta_{\max} = \{0.05, 0.15\}$ sec. The impact of equipment failure is dominant for lower values of ρ , and has minimal effect otherwise. In these regions, the impact of the MTTR value is also importance. (Bottom) The holistic resilience of the BH network with $\rho = 3$ dB and $\Delta_{\max} = 0.1$ sec; comparison between Rice fading ($K = 10$) and Rayleigh Fading ($K = 0$).

gateways in layer 2 and the core network has a cumulative mean delay of 10 msec[3]. The parameters employed to model the wireless links' capacity, latency, and resilience are listed in Table III, in which we consider a microwave band operating in the 38 GHz spectrum. The expected capacity of a last-mile wireless microwave hop that exhibits LOS fading is derived using (12). The expectations of delay and resilience in microwave links are based on (18) and (23), respectively. We adopt the network topology that was presented in Figure 1 and which consists of two hops. The first is the last-mile connecting the small cells to an aggregation point and uses either microwave links or fibre-based links (with mean capacity of 10 Gbps). The second hop connects the aggregation point to the gateway in the core network and is always provisioned with fibre-based links (10 Gbps). We study the impact of increasing the density of aggregation points and/or the proportion of

[3]Assuming the BH gateway to the core network has similar processing delay parameters to the gateway in layer 2 and 99 connected lines, the delay can be computed as: $5 \cdot (1 + 99) \times (5 + 0.01 \cdot 1500) = 10$ msec

TABLE II
SIMULATION PARAMETERS.

Parameter	Value	Remark
λ_0	400 users/km^2	Density of Φ_0 PPP representing users.
λ_1	40 cells/km^2	Density of Φ_1 PPP representing small cells.
λ_2	4 gateways/km^2	Density of Φ_2 PPP representing BH aggregation points.
λ_3	1 gateway/km^2	Density of Φ_3 PPP representing BH gateways.
p_m	50%	50% of last-mile links are randomly allocated microwave (38 GHz) technology.
p_f	50%	50% of last-mile links are randomly allocated fibre-based technology.

TABLE III
PERFORMANCE MODELLING PARAMETERS IN ADDITION TO THOSE LISTED IN TABLE I.

Parameter	Value	Remark
ϕ_3^f	5	Scalar factor representing the processing power of BH gateway (lower value indicates better processing power).
ϕ_2^f	10	Scalar factor representing the processing power of fibre aggregation point.
ϕ_2^m	10	Scalar factor representing the processing power of microwave aggregation point.
a_3^f	5 μsec	Traffic-independent processing delay of BH gateway.
a_2^f	10 μsec	Traffic-independent processing delay of fibre aggregation point.
a_2^m	10 μsec	Traffic-independent processing delay of microwave aggregation point.
b_3^f, b_2^f, b_2^m	0.01 μsec/bit	Processing delay of all routers relative to the packet size.
ϵ	1500 bits	Ethernet packet size.

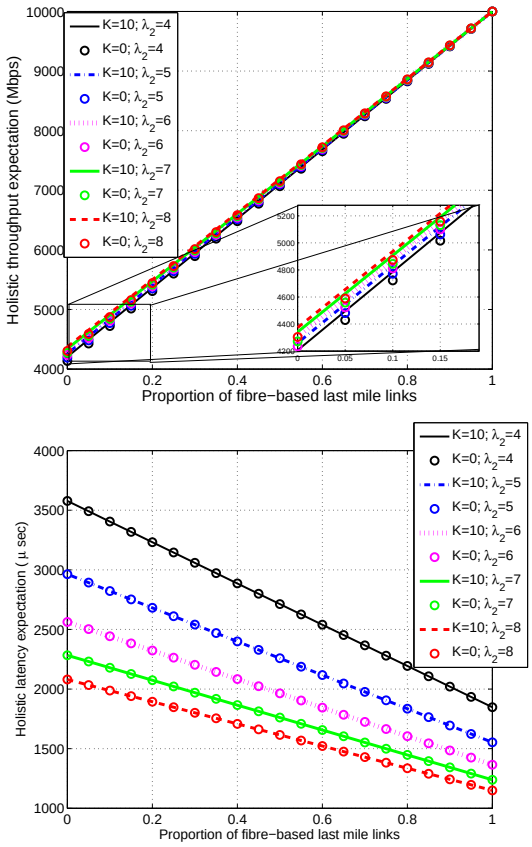

Fig. 10. Holistic BH network throughput (top) and latency (bottom) for LOS-fading with $K = 10$ and Rayleigh fading with $K = 0$.

fibre-based last-mile links on the holistic BH performance. In parallel, we compare the results with both Rice and Rayleigh fading considerations.

We vary the proportion of last-mile fibre links and the density of the aggregation gateways in layer 2 and examine the resulting impact on the expectations of the multi-hop BH throughput and latency in Figures 10 (Top) and (Bottom), respectively. The node density λ_2 has limited effect on the resulting holistic throughput, whereas the increase of fibre links steps up the throughput by a factor of two. In contrast, the increase of node density λ_2 (i.e., proportion of fibre last-mile links) have equal share in reducing the holistic latency of the multi-hop BH. As for resilience, the impact of increasing the share of fibre in the last mile doubles the resilience of the BH network, as seen in Figure 9 (Bottom).

Had Rayleigh fading ($K = 0$) been considered instead of LOS-fading (e.g., $K = 10$), the resulting capacity estimation would be pessimistic as clearly seen in the zoom-in window of Figure 10 (Top). Whereas, the type of fading does not have a significant impact on the latency, as expected from the results obtained in in Section III-B. Essentially, the delay in the holistic BH link is dominated by the processing and queuing delays, as such, the difference in delay caused by the error in modelling the fading is negligible. In contrast, resilience of wireless links is the most vulnerable to the type of fading, as seen in Figure 9 (Bottom). Consequently, the error in adopting Rayleigh fading models instead of Rice fading when estimating the multi-hop BH resilience is significant and would result in invalid conclusions.

V. USER-CENTRIC-BH OPTIMISATION PROBLEM

The User-Centric-Backhaul (UCB) is the state-of-the-art user-cell association scheme that is radio-aware, BH-aware, and user-centric at the same time [26]. The UCB uses multiple

offset values that are optimised per cell, where each offset reflects the end-to-end characteristics of that cell with respect to quality attribute, e.g., capacity, latency, resilience, etc. On the other hand, each user has different quality targets that are determined by the device capabilities, the application, and the user's preferences. For instance, a delay-critical e-health user would have stringent latency but relaxed throughput requirements. A streaming application may have the opposite priorities, whereas a security sensor demands ultra-high reliability ($> 99.999\%$ availability). The UCB allows users to make a judicious cell selection that is aware of the candidate cells' end-to-end characteristics (as opposed to radio conditions only) and of the users' specific needs. In other words, two users having the same signal reception of all surrounding cells may choose differently according to their disparate quality targets. Similarly, two cells with exactly the same radio characteristics, may have unequal offset values due to dissimilar limitations on their respective BH links.

In this section, we develop an analytical solution to a subproblem of the UCB, the throughput-based UCB (T-UCB), which is concerned with one BH link per cell and a single attribute: Throughput. We consider a mono-layer network of small cells that have identical radio characteristics and that have a purposely over-dimensioned radio access. Each of these cells connects to the BH gateway using the topology described in the previous section. Effectively, there are two types of small cells: C_f with fibre-based last-mile and C_m with microwave-based last-mile. Such a network can be modelled, using a stationary mixed PPP Φ_1 with a randomized intensity function H having a two-point distribution such that:

$$\Pr(\mathrm{H} = \lambda_m) = p_m,\ \Pr(\mathrm{H} = \lambda_f) = p_f = 1 - p_m, \quad (24)$$

where, $0 < p_m < 1$ is the probability of having a cell of type C_m and p_f is the probability of having a cell of type C_f. Hence, the intensity of Φ_1 is $\lambda = p_m\lambda_m + (1-p_m)\lambda_f$, where $\lambda_m > 0$ is the intensity of cells of type C_m and $\lambda_f > 0$ is the intensity of cells of type C_f. The adoption of PPP in the representation of small cells locations is justified since such randomness may be expected in small cells' deployment.

Let the users be also located according to a homogeneous PPP Φ_0 with intensity λ_0 that is independent of Φ_1. We denote the variable R as the distance separating the typical/random user located at the origin, without loss of generality, from the closest cell in Φ_1. The T-UCB optimisation problem consists of finding the optimum association policy $\mathcal{A}(O_m, O_f) = [\mathcal{A}_m(O_m, O_f), \mathcal{A}_f(O_m, O_f)]$ that would maximise the ergodic throughput without exceeding the capacity limits of both types of BH links, $\mathrm{E}\{T_m\}$ and $\mathrm{E}\{T_f\}$. The factors $\mathcal{A}_m$ and $\mathcal{A}_f$ represent the proportion of users associated to cells of type C_m and C_f, respectively. The association policy is a function of the offset settings in both cell types (O_m, O_f) that can take on any positive value. The BH capacity constraints are (26) and (27), which dictate that the SINR-based throughput ($\dot{T}_m$ and $\dot{T}_f$) of all served users ($\mathcal{N}_m$ and $\mathcal{N}_f$) affected by the overhead G_m and G_f, should not exceed the nominal capacities $\mathrm{E}\{T_m\}$ and $\mathrm{E}\{T_f\}$, respectively.

$$\max_{\mathcal{A}} \dot{T}(\mathcal{A}) = \mathcal{A}_m\dot{T}_m(\mathcal{A}) + \mathcal{A}_f\dot{T}_f(\mathcal{A}) \quad (25)$$

subject to

$$\mathrm{E}\{T_m\} - \mathcal{N}_m\dot{T}_m \times G_m \geq 0 \quad (26)$$

$$\mathrm{E}\{T_f\} - \mathcal{N}_f\dot{T}_f \times G_f \geq 0 \quad (27)$$

The ergodic throughput pertaining to the traditional user-cell association policy is derived in many works that also employ stochastic geometry to capture the network topology (e.g., [9]). The T-UCB association policy, however, results in a new distribution of the distance between user and serving cell, since it is not necessarily the closest. The received signal power is a function of that distance, and the throughput is a function of the received signal power of serving and all interfering cells.

In order to solve the optimisation problem, we need to first derive the analytical expression for the system throughput, assuming the following two variables: (i) offset setting per cell type, and (ii) distance between a typical user and the serving cell. The distance is conditioned on the association policy, thus, is a function of the offset value. We first formulate the association policy in Section V-A. Next, we determine the distribution of the distance between a typical user and the corresponding serving cell (based on the association policy) in Section V-B. Finally, we find the ergodic throughput in Section V-C.

A. Basic UCB association policy

The cell association of a typical user U_u in a UCB system is based on the maximum *biased* mean received power (or rank) from all cells C_c as defined in (28), given that all cells have the same power per user, P_a, and the same propagation characteristics (α_a and χ_a). It should be noted that, in this problem, there are two wireless links with very different characteristics. The first is the wireless *BH* which is characterised by LOS fading and is often noise limited. The second is the radio *access* between the cell and the users which is often none LOS and interference limited [9]. To this end, we use the subscript $_a$ to differentiate the propagation parameters of the radio *access* link from those of the wireless *BH*):

$$\mathcal{R}_{u,c} = \mathrm{E}\{J_{c,u}\} \times O_c = P_a \cdot \chi_a \cdot {R_{u,c}}^{-\alpha_a}; \forall c = \{m, f\}. \quad (28)$$

Cell association often is based on mean received power (as opposed to instantaneous values) in order to avoid ping-pong effect that may result if fading were accounted for. The probability of a typical user associating with a cell C_c is thus equivalent to the probability of $\mathcal{R}_{u,c} > \mathcal{R}_{u,n}$ for all other cells C_n. In a T-UCB, a typical user either connects to cell type C_m or C_f, based on the association policy $\mathcal{A} = [\mathcal{A}_m, \mathcal{A}_f]$.

Theorem V.1. *The probability of a typical user attaching to*

cell C_m or C_f can be expressed as follows:

$$\mathcal{A}_m = \frac{1}{\left(\frac{O_f}{O_m}\right)^{2/\alpha}+1} \quad (29)$$

$$\mathcal{A}_f = \frac{1}{\left(\frac{O_m}{O_f}\right)^{2/\alpha}+1}. \quad (30)$$

Proof: *The proof is provided in Appendix D.*

B. Policy-based user-cell distance

The minimum distance between a typical user and a cell is a variable R as explained in Section II-B. However, with T-UCB association policy, the serving cell is not necessarily the closest. We consider a typical user at the origin associated with a cell of type C_m or C_f. Denote X_m (or X_f) as the distance between the user and its serving cell. Since cells are deployed as a PPP, X_m and X_f are random variables described by their probability density function $f_{X_m}(x)$ and $f_{X_f}(x)$ that we derive in this section. We first define the ccdf $\overline{F}_{X_m}(x)$, as follows:

$$\overline{F}_{X_m}(x) \triangleq \Pr\left(R_m > x | c = m\right) = \frac{\Pr\left(R_m > x, c = m\right)}{\Pr\left(c = m\right)}. \quad (31)$$

Lemma V.2. *The complementary cumulative distribution function that represent the variable distance between the typical user and a cell of type C_m can be expressed as follows:*

$$\overline{F}_{X_m}(x) = e^{\frac{-\pi\lambda x^2}{\mathcal{A}_m}}. \quad (32)$$

Proof: *The proof is provided in Appendix E.*

Consequently, the pdf of the policy-based user-cell distance can be found as follows:

$$f_{X_m}(x) = \frac{\mathrm{d}F_{X_m}(x)}{\mathrm{d}x} = \frac{\mathrm{d}(1-\overline{F}_{X_m}(x))}{\mathrm{d}x} = \frac{2\pi\lambda}{\mathcal{A}_m} x \cdot e^{-x^2\left(\frac{\pi\lambda}{\mathcal{A}_m}\right)}. \quad (33)$$

Similarly, $f_{X_f}(x)$ can be obtained as follows:

$$f_{X_f}(x) = \frac{2\pi\lambda}{\mathcal{A}_f} x \cdot e^{-x^2\left(\frac{\pi\lambda}{\mathcal{A}_f}\right)}. \quad (34)$$

C. Ergodic throughput

In this section, we derive the average ergodic throughput $\dot{T}$ of a typical user that has $\mathcal{A}_f$ probability of connecting to a cell of type C_f and $\mathcal{A}_m$ otherwise.

$$\dot{T} = \mathcal{A}_f \cdot \dot{T}_f + \mathcal{A}_m \cdot \dot{T}_m, \quad (35)$$

where, $\dot{T}_m$ and $\dot{T}_f$ are the average throughput of a typical user associated with cell type C_m and C_f, respectively. The average throughput over a radio access channel bandwidth W_a is $\dot{T}_c(x, \gamma'(x)) \triangleq \mathrm{E}\left\{\mathrm{E}\left\{\mathrm{W}_a \log_2\left(1+\gamma'(x)\right) \mid x\right\}\right\}$. It is a function of two variables: the distance between user and associated cell (x) and the received SINR (γ'). The SINR of a typical user at a random distance x from its associated cell C_c is shown in (36). The expression $\mathrm{E}\left\{\mathrm{W}_a \log_2\left(1+\gamma'(x)\right) \mid x\right\}$ is the distribution of the instantaneous throughput conditioned to a particular value x. It is derived in [9], assuming that the power of fading of both serving and interfering channels are exponentially distributed with unit mean, as in (37). Where, τ_a is the target throughput, γ is the signal-over-noise ratio (SNR), and $\mathcal{L}$ is the Laplace function as defined in (38).

For a p articular case in which the radio coverage is interference limited, the SINR can be approximated with the signal-to-interference ratio ($\mathrm{SIR} = \dot{\gamma}$) (i.e., $\sum_{i \neq c} J_{i,u} \gg N_{th}$). If, in addition, we assume that $\alpha_a = 4$, the expected throughput at a given distance can be further simplified as in (39) [9]. The general average ergodic throughput based on two variables: x and γ' may be obtained by replacing the derived expressions (37) and (33), as shown in (40). For the particular interference-limited scenario with $\alpha_a = 4$, expression (40) can be further simplified, as in (41). Plugging (41) in (35), we get the average ergodic throughput of a typical user in the network (for the interference-limited basic deployment with $\alpha_a = 4$), as shown in (42). The average number of users associated with cells of type $c = [m, f]$ can be obtained as the ratio $\mathcal{N}_c = \mathcal{A}_c \cdot \lambda_0 / \lambda_c$, where λ_0 is the intensity of the users' PPP and λ_c is the density of cells' PPP (Φ_1). Accordingly, the average throughput of a cell of type C_c can be expressed as in (43) (for the special case).

D. Results and Analysis

In this section, we solve the T-UCB optimisation problem using an exhaustive search approach. We consider the special case of interference-limited radio access together with a propagation exponent $\alpha_a = 4$. The remaining parameters are listed in Table IV. The expected throughput capacity of the microwave link can, thus, be derived using the expression in (12) which equates to 160.75 Mbps. The last-mile fibre throughput capacity is considered to be 1 Gbps. We plot the objective function (25) and the constraints (26) and (27) for all possible values of $\mathcal{A}_m$ (note that $\mathcal{A}_f = 1 - \mathcal{A}_m$). We assume that $\lambda_m = \lambda_f = 40$ cells per km^2 and $\lambda_1 = p_m \cdot \lambda_m + (1 - p_m) \cdot \lambda_f = 40$ cells per km^2 with $p_m = 0.5$ and $\lambda_0 = 1200$ users per km^2. The y-axis shows the network load and the unused BH load (a nil value indicates 100% usage of the BH available capacity, a negative value means

TABLE IV
PARAMETERS EMPLOYED TO OBTAIN EXPERIMENTAL RESULTS; REMAINING PARAMETERS ARE DEFINED IN TABLE I.

Parameter	range
λ_2 (gateways/km^2)	4 to 40
λ_1 (cells/km^2)	40
p_m	0 to 1
λ_0 (users/km^2)	1200
$G_f = G_m$	0.3
MIMO rank	2
α_a	4
α	2.5
P	10dBm+18dBi
A	18dBi

$$\gamma'(x) = \frac{J_{c,u}}{N_{th} + \sum_{i \in \phi_c \setminus c} (J_{i,u})} = \frac{\mathrm{E}\{J_{c,u}\} \cdot h_{c,u}}{N_{th} + \sum_{i \in \phi_c \setminus c} (\mathrm{E}\{J_{c,u}\} \cdot h_{i,u})}. \tag{36}$$

$$\mathrm{E}\left\{\mathrm{W}_a \log_2\left(1+\gamma'(x)\right) \mid x\right\} = \mathrm{W}_a \ln 2 \int_0^\infty \exp\left\{ -\frac{2^{\tau_a}-1}{\gamma} \right\} \times \mathcal{L}_{I_x}(x^\alpha (2^{\tau_a}-1)) d\tau_a, \tag{37}$$

$$\mathcal{L}_{I_x}(x^{\alpha_a}(2^{\tau_a}-1)) = \exp\left(-\pi\lambda x^2 (2^{\tau_a}-1)^{2/\alpha_a} \int_{(2^{\tau_a}-1)^{-2/\alpha}}^\infty \frac{1}{1+u^{\alpha_a/2}} du \right). \tag{38}$$

$$\begin{aligned} \mathrm{E}\left\{\mathrm{W}_a \log_2\left(1+\dot{\gamma}(x)\right) \mid x\right\} &= \mathrm{W}_a \ln 2 \int_{\tau_a>0} \mathcal{L}_{I_x}(x^4 (2^{\tau_a}-1)) d\tau_a \\ &= \mathrm{W}_a \ln 2 \int_{\tau_a>0} e^{-\pi\lambda x^2 \sqrt{2^{\tau_a}-1}\left(\frac{\pi}{2} - \arctan\left(\frac{1}{\sqrt{2^{\tau_a}-1}}\right)\right)} d\tau_a. \end{aligned} \tag{39}$$

$$\begin{aligned} \dot{T}_c &= \int_0^\infty \mathrm{E}\left\{\mathrm{W}_a \log_2\left(1+\gamma(x)\right) \mid x\right\} \times f_{X_c}(x) dx \\ &\frac{2\pi\lambda}{\mathcal{A}_c} \mathrm{W}_a \ln 2 \int_0^\infty \int_0^\infty e^{-\pi\lambda \frac{x^2}{\mathcal{A}_c}} \exp\left\{ -\frac{2^{\tau_a}-1}{\gamma} \right\} \cdot \mathcal{L}_{I_x}(x^{\alpha_a}(2^{\tau_a}-1)) d\tau_a x dx. \end{aligned} \tag{40}$$

$$\begin{aligned} \dot{T}_c\left(\alpha_a = 4, \gamma' \sim \dot{\gamma}\right) &= \frac{2\pi\lambda}{\mathcal{A}_c} \times \mathrm{W}_a \ln 2 \int_0^\infty \int_0^\infty e^{-\pi\lambda \frac{x^2}{\mathcal{A}_c}} \times e^{-\pi\lambda x^2 \sqrt{2^{\tau_a}-1}\left(\frac{\pi}{2} - \arctan\left(\frac{1}{\sqrt{2^{\tau_a}-1}}\right)\right)} x dx d\tau_a \\ &= \mathrm{W}_a \ln 2 \int_0^\infty \frac{1}{1 + \mathcal{A}_c \times \sqrt{2^{\tau_a}-1}\left(\frac{\pi}{2} - \arctan\left(\frac{1}{\sqrt{2^{\tau_a}-1}}\right)\right)} d\tau_a. \end{aligned} \tag{41}$$

$$\dot{T}\left(\alpha_a = 4, \gamma' \sim \dot{\gamma}\right) = \mathrm{W}_a \ln 2 \sum_{c=\{m,f\}} \int_0^\infty \frac{\mathcal{A}_c}{1 + \mathcal{A}_c \times \sqrt{2^{\tau_a}-1}\left(\frac{\pi}{2} - \arctan\left(\frac{1}{\sqrt{2^{\tau_a}-1}}\right)\right)} d\tau_a. \tag{42}$$

$$\begin{aligned} \dot{T}^c &= \mathcal{N}_c \times \dot{T}_c \\ &= \frac{\mathcal{A}_c \cdot \lambda_0}{\lambda_c} \times \mathrm{BW} \ln 2 \int_0^\infty \frac{1}{1 + \mathcal{A}_c \times \sqrt{2^{\tau_a}-1}\left(\frac{\pi}{2} - \arctan\left(\frac{1}{\sqrt{2^{\tau_a}-1}}\right)\right)} d\tau_a. \end{aligned} \tag{43}$$

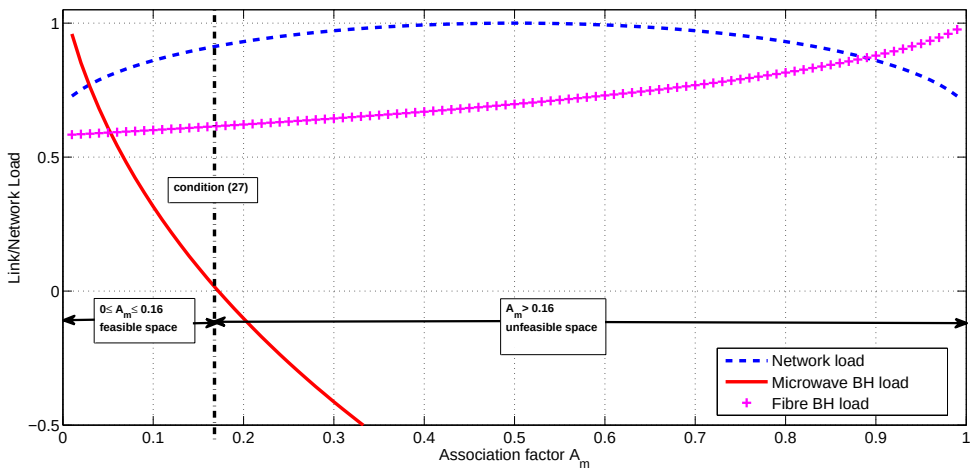

Fig. 11. Exhaustive search solution for the T-UCB problem. The link load shown represents the unused proportion of the nominal link capacity; negative values indicate overload and positive values reflect unused capacity.

the BH is overloaded, and a positive value indicates the available unused BH capacity). The resulting curves are shown in Figure 11 and the solution space is demarcated by the condition (26). The limiting condition defined by (27) is never reached, in this scenario, and the optimum association policy is $\mathcal{A}^* = [0.16, 0.84]$.

A BH-unaware association scheme would have resulted in equal share of users between both cell types and would have incurred overload of the wireless BH cells by about 88%. Such a BH condition would reflect on the quality perceived by half of the users who would be suffering from queuing delays, lost packets, and significant reduction in throughput. If we normalise the effect of BH overload on all users attached to cells of type C_m, then each would experience a throughput reduction equal to $(0.88 \times 160.75)/(\mathcal{N}_m) = 9.43$ Mbps for $\mathcal{N}_m = 15$ users per cell.

1) Sensitivity analysis: In this section, we study the effect of key parameters on the optimisation results. The effect of the probability p_m of cells of type C_m is first studied in Figure 12 (Top), assuming the same cells and users densities as in the previous section. As expected, more users associate with the fibre-based cells when these increase in density. Moreover, the optimum curve deviates from the linear relationship due to the constraint determined by the wireless BH capacity, which in this figure is calculated based on $\lambda_2 = 4$ aggregation points per km^2, i.e., 160.75 Mbps. The highest association factor with cells of type C_m is 0.4 and occurs when the proportion of such cells is 85%. There are no feasible solutions beyond this value that would satisfy the microwave capacity constraint.

Next, we inspect the effect of the wireless BH capacity on the association policy in Figure 12 (Bottom), where the probability of cells of type C_m is $p = 0.5$. For values of $\lambda_2 \geq 13$ aggregation points per km^2 (i.e., 307.2 Mbps), the network becomes radio access limited and the increase in microwave capacity does not affect the association policy.

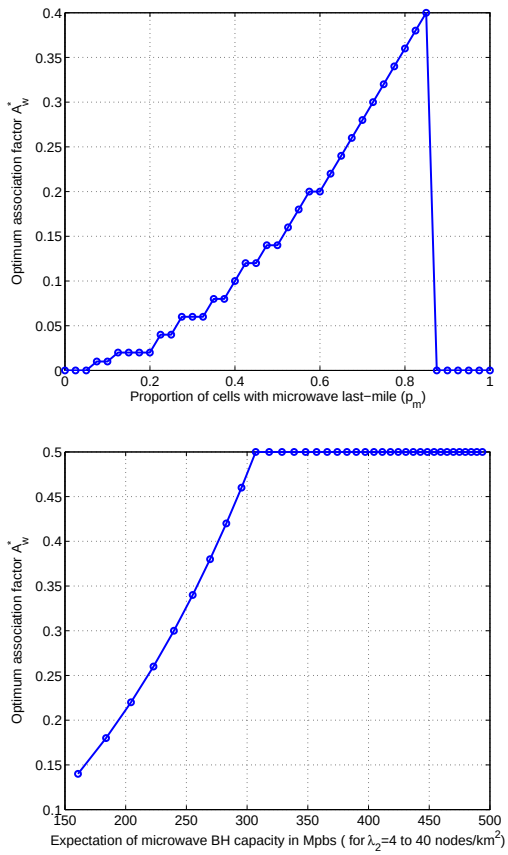

Fig. 12. (Top) The effect of microwave cell density on the association policy. (Bottom) The effect of microwave BH capacity on the association policy.

VI. Conclusion

We have presented in this article tractable models that capture three key performance characteristics of wireless BH links: throughput, latency, and resilience. This is the first work that offers analytical performance models that are representative of the BH-specific LOS nature of wireless propagation. The derived expressions are employed as a modular part of the multi-hop hybrid BH performance modelling. Moreover, an association scheme that is aware of the performance of the multi-hop BH links (including wireless hops) is elaborated and shown to improve user-centric performance.

Appendix A

Proof: The average throughput of a wireless link at a given distance x is derived here, starting with the pdf of Rice fading:

$$f_{\gamma_x}(z) = \frac{1+K}{\Omega_x} e^{-\frac{z(1+K)}{\Omega_x}} e^{-K} I_0\left(2\sqrt{\frac{z}{\Omega_x}K(K+1)}\right), \tag{44}$$

Plugging (44) into (8), the integral can be solved as previously done by using the result in [27, eq. 5] and after some simple manipulation as in [28, eq. 6], the expression in (9) can be found and the proof is complete. ■

Appendix B

Proof: The average throughput of a wireless link at a given distance x is derived here using the fluctuating Rice fading channel model. By restricting the parameter m to take positive integer values, the distribution of γ_x is given in a very simple form [17], [18] as:

$$f_{\gamma_x}(z) = \sum_{i=0}^{m-1} C_i \cdot \frac{1}{B_x^{m-i}} \frac{z^{m-1-i}}{(m-i)!} e^{-\frac{z}{B_x}}, \tag{45}$$

with $B_x \triangleq \Omega_x(m+K)/m(1+K)$ and C_i as defined in Section II-A. Plugging (45) into (8), and using ([18, eq. 23]), we find an approximate expression for the average rate T_x as in (10) and the proof is complete. ■

Appendix C

Proof: The average throughput of a wireless link, $\mathrm{E}\{T\}$, taken over both the variable distance and fading component can be approximated by using (11) to represent the upper incomplete Gamma function $\Gamma(-l, z)$ and replacing $z = x^2/B$,

$$\mathrm{E}\{T\} \approx \frac{W}{\ln(2)} \sum_{i=0}^{m-1} C_i \sum_{l=0}^{m-i-1} \pi\lambda B \int_0^{\infty} e^{z} \cdot z^{l} \cdot \Gamma\left(-l, z\right) \cdot e^{-\pi\lambda B z} dz,$$

$$\mathrm{E}\{T\} \approx \frac{W}{\ln(2)} \sum_{i=0}^{m-1} C_i \sum_{l=0}^{m-i-1} \pi\lambda B \frac{(-1)^{l}}{l!} \int_0^{\infty} z^{l} \cdot e^{(1-\pi\lambda B)z} \cdot \left[E_1\left(z\right) - e^{-z} \sum_{r=0}^{l-1} (-1)^{r} \frac{r!}{z^{r+1}} \right] dz,$$

$$\approx \frac{W}{\ln(2)} \sum_{i=0}^{m-1} C_i \sum_{l=0}^{m-i-1} \pi\lambda B \frac{(-1)^{l}}{l!} \left\{ I_1 + I_2 \right\}. \tag{46}$$

as in (46). Thus, solving (46) equates to solving the following two integrals:

$$I_1 = \int_0^{\infty} e^{\eta \cdot z} z^{l} \cdot E_1\left(z\right) dz. \tag{47}$$

$$I_2 = -\int_0^{\infty} e^{(\eta-1)z} z^{l} \sum_{r=0}^{l-1} (-1)^{r}\, r! \cdot z^{-r-1} dz. \tag{48}$$

with $\eta \triangleq 1 - \pi\lambda B$.

We first solve I_1 using [29, eq. 21 p. 198]. Note that, in this case, $\Gamma(\cdot)$ is the Gamma function which is equivalent to $\Gamma(y) = (y-1)!$.

$$I_1 = \int_0^{\infty} e^{\eta z} z^{l} E_1\left(z\right) dz,$$
$$= \frac{\Gamma(l+1)}{l+1} {}_2F_1\left(l+1, l+1; l+1; 1-\pi\lambda B\right). \tag{49}$$

The second integral I_2 can be re-arranged, as follows, with a direct solution using the Gamma function.

$$I_2 = -\sum_{r=0}^{l-1} (-1)^{r}! \int_0^{\infty} z^{l-r-1} e^{-\pi\lambda B z} dz$$
$$= -\sum_{r=0}^{l-1})(-1)^{r} r! (\pi\lambda B)^{r-l} \Gamma(l-r)$$
$$= -\sum_{r=0}^{l-1} (-1)^{r} r! (\pi\lambda B)^{r-l} (l-r-1)! \tag{50}$$

By replacing I_1 and I_2 by (49) and (50), respectively, in (46), the expression (12) is obtained, and the proof is complete. ■

APPENDIX D

Proof: The probability of a typical user associating with cell of type C_m is A_m and is defined as follows:

$$\begin{aligned}
\mathcal{A}_m &\triangleq \Pr[c=m] = \mathrm{E}_{R_m}\left[\Pr\left[\mathcal{R}_m(R_m) > \mathcal{R}_f\right]\right] \\
&\overset{(a)}{=} \mathrm{E}_{R_m}\left[\Pr\left[R_f > \left(\frac{O_f}{O_m}\right)^{1/\alpha_a} \times R_m\right]\right] \\
&= \int_0^{\infty} \Pr\left[R_f > \left(\frac{O_f}{O_m}\right)^{1/\alpha_a} \times R_m\right] \times f_{R_m}(r) dr \\
&\overset{(b)}{=} \int_0^{\infty} e^{-\pi\lambda\left(\frac{O_f}{O_m}\right)^{2/\alpha_a} \times r^2} \times 2\pi\lambda \cdot r \cdot e^{-\pi\lambda r^2} dr \\
\mathcal{A}_m &\overset{(c)}{=} \frac{1}{\left(\frac{O_f}{O_m}\right)^{2/\alpha_a} + 1}.
\end{aligned} \tag{51}$$

The equality (a) is a direct result of replacing $\mathcal{R}$ by the expression in (28) and (b) follows from using ccdf expression $\overline{F}_R(r)(r) = \exp(-\pi\lambda r^2)$. The final result (c) is obtained by replacing $y = r^2$ and a straight forward integration. The association probability with cell of type C_f can be obtained in a similar manner as:

$$\mathcal{A}_f = \frac{1}{\left(\frac{O_m}{O_f}\right)^{2/\alpha_a} + 1}. \tag{52}$$

It can be verified that $\mathcal{A}_m + \mathcal{A}_f = 1$, and the proof is complete. ■

APPENDIX E

The complementary cumulative distribution function that represent the variable distance between the typical user and a cell of type C_m is derived here.

Proof: The probability $\Pr\left[s=m\right]$ is equal to $\mathcal{A}_m$, as shown in Section V-A. The joint probability $\Pr\left[R_m > x, s=m\right]$ can be found as follows:

$$\begin{aligned}
\Pr\left[R_m > x, s=m\right] &= \Pr\left[R_m > x, \mathcal{R}_m(R_m) > \mathcal{R}_f\right] \\
&= \int_x^{\infty} \Pr\left[\mathcal{R}_m(r) > \mathcal{R}_f\right] f_{R_m}(r) dr \\
&= 2\pi\lambda \int_x^{\infty} r \cdot e^{-\pi\lambda r^2 \left(\left(\frac{O_f}{O_m}\right)^{2/\alpha_a} + 1\right)} dr \\
&= \mathcal{A}_m \cdot e^{\frac{-\pi\lambda x^2}{\mathcal{A}_m}}.
\end{aligned} \tag{53}$$

Plugging (53) into (31) leads to the expression (32), and the proof is complete. ■

REFERENCES

[1] P. Marshall, "5G Operator survey," tech. rep., The Telecommunications Industry Association (TIA), Jan. 2017.
[2] M. Jaber, M. Imran, R. Tafazolli, and A. Tukmanov, "5G backhaul challenges and emerging research - A survey," *IEEE Access*, vol. 4, no. 2016, pp. 1–1, 2016.
[3] W. Coomans, R. B. Moraes, K. Hooghe, A. Duque, J. Galaro, M. Timmers, A. J. van Wijngaarden, M. Guenach, and J. Maes, "XG-FAST: Towards 10 Gb/s copper access," in *IEEE Globecom Workshops (GC Wkshps)*, pp. 630–635, Dec 2014.
[4] R. Van Uden, R. A. Correa, E. A. Lopez, F. Huijskens, C. Xia, G. Li, A. Schülzgen, H. De Waardt, A. Koonen, and C. Okonkwo, "Ultra-high-density spatial division multiplexing with a few-mode multicore fibre," *Nature Photonics*, vol. 8, no. 11, pp. 865–870, 2014.
[5] M. Coldrey, "Maturity and field proven experience of millimetre wave transmission," white paper, ETSI- European Telecommunications Standards Institute, 2015.
[6] G. Paschos, E. Bastug, I. Land, G. Caire, and M. Debbah, "Wireless caching: technical misconceptions and business barriers," *IEEE Communications Magazine*, vol. 54, pp. 16–22, Aug. 2016.

[7] X. Costa-Perez, A. Garcia-Saavedra, X. Li, T. Deiss, A. de la Oliva, A. di Giglio, P. Iovanna, and A. Moored, "5G-Crosshaul: An SDN/NFV integrated fronthaul/backhaul transport network architecture," *IEEE Wireless Communications*, vol. 24, pp. 38–45, Feb. 2017.
[8] Ericsson, "Microwave towards 2020, white paper." [Online], Available: https://www.ericsson.com/res/docs/2015/, Accessed on 30/06/2016, 2015.
[9] J. Andrews, F. Baccelli, and R. Ganti, "A tractable approach to coverage and rate in cellular networks," *IEEE Transactions on Communications*, vol. 59, pp. 3122–3134, Nov. 2011.
[10] M. Jaber, M. Imran, A. Sutton, A. Tukmanov, and R. Tafazolli, "Modular approach for modelling the hybrid multi-hop backhaul performance," *IEEE Wireless Communications Letters*, vol. 6, no. 2, pp. 262–265, 2017.
[11] D. C. Chen, T. Q. S. Quek, and M. Kountouris, "Wireless backhaul in small cell networks: Modelling and analysis," in *IEEE 79th Vehicular Technology Conference (VTC Spring)*, pp. 1–6, May 2014.
[12] D. C. Chen, T. Q. S. Quek, and M. Kountouris, "Backhauling in heterogeneous cellular networks: Modeling and tradeoffs," *IEEE Transactions on Wireless Communications*, vol. 14, pp. 3194–3206, June 2015.
[13] G. Zhang, T. Quek, A. Huang, M. Kountouris, and H. Shan, "Delay modeling for heterogeneous backhaul technologies," in *IEEE 82nd Vehicular Technology Conference (VTC Fall)*, pp. 1–6, Sept 2015.
[14] G. Zhang, T. Quek, M. Kountouris, A. Huang, and H. Shan, "Fundamentals of heterogeneous backhaul design - analysis and optimization," *IEEE Transactions on Communications*, vol. 64, no. 2, pp. 876 – 889, 2016.
[15] D. Ohmann and G. P. Fettweis, "Minimum duration outage of wireless Rayleigh-fading links using selection combining," in *IEEE Wireless Communications and Networking Conference (WCNC)*, pp. 681–686, Mar. 2015.
[16] J. M. Romero-Jerez, F. J. Lopez-Martinez, J. F. Paris, and A. J. Goldsmith, "The fluctuating two-ray fading model: Statistical characterization and performance analysis," *IEEE Transactions on Communications*, vol. 16, pp. 4420–4432, July 2017.
[17] J. Paris, "Closed-form expressions for Rician shadowed cumulative distribution function," *Electronics Letters*, vol. 46, pp. 952–953, June 2010.
[18] F. J. Lopez-Martinez, J. F. Paris, and J. M. Romero-Jerez, "The κ-μ shadowed fading model with integer fading parameters," *IEEE Transactions on Vehicular Technology*, vol. 66, no. 9, pp. 7653–7662, 2017.
[19] S. Singh, M. N. Kulkarni, A. Ghosh, and J. G. Andrews, "Tractable model for rate in self-backhauled millimeter wave cellular networks," *IEEE Journal on Selected Areas in Communications*, vol. 33, pp. 2196–2211, Oct 2015.
[20] I. S. Gradshteyn and I. M. Ryzhik, *Table of Integrals, Series and Products*. 7th ed., 2007.
[21] M. K. Simon, *Probability distributions involving Gaussian random variables: A handbook for engineers and scientists*. Springer Science & Business Media, 2007.
[22] R. Nadiv and T. Rosenhouse, "Flex your backhaul network with adaptive coding & modulation." [Online], Available: http://www.winncom.com/, Accessed 07/11/2016, 2010.
[23] G. Stuber, *Principles of Mobile Communication*. Kluwer Academic Publishers, 2nd Edition, 2nd ed., 2001.
[24] S. O. Rice, "Distribution of the duration of fades in radio transmission: Gaussian noise model," *The Bell System Technical Journal*, vol. 37, pp. 581–635, May 1958.
[25] F. Ramos-Alarcon, V. Kontorovich, and M. Lara, "On the level crossing duration distributions of Nakagami processes," *IEEE Transactions on Communications*, vol. 57, pp. 542–552, February 2009.
[26] M. Jaber, M. Imran, R. Tafazolli, and A. Tukmanov, "A distributed SON-based user-centric backhaul provisioning scheme," *IEEE Access*, vol. 4, pp. 2314 – 2330, May 2016.
[27] N. C. Sagias, G. S. Tombras, and G. K. Karagiannidis, "New results for the Shannon channel capacity in generalized fading channels," *IEEE Communications Letter*, vol. 9, pp. 97–99, Feb 2005.
[28] D. B. D. Costa and M. D. Yacoub, "Average channel capacity for generalized fading scenarios," *IEEE Communications Letter*, vol. 11, pp. 949–951, December 2007.
[29] M. Geller and E. W. Ng, "A table of integrals of the exponential integral," *JOURNAL OF RESEARCH of the National Bureau af Standards - B. Mathematics and Mathematical Science*, vol. 73B, pp. 191–210, July-September 1969.